



12 September 2024
inanc.arda@outlook.com
arda.inanc@cern.ch

Particle Tracking for FCC-ee Top-up Injection

A. İnanç, Y.Dutheil, S.Yue
CERN, CH-1211 Geneva, Switzerland

Keywords: FCC-ee, collider injection, particle tracking, Xsuite

Abstract

FCC-ee (Future Circular e^+e^- Collider) is the next generation highest-luminosity energy frontier lepton collider, designed to deliver record luminosity for the precision studies of Z, W, H and t. To maintain the stored beam current and maximize luminosity throughout the physics run, top-up injection scheme is needed for the collider. In this study several aspects of FCC-ee collider top-up injection (such as injection efficiency, dynamic aperture, momentum acceptance, nonlinear dispersion, on-axis injection and hybrid on-off axis injection, twiss parameter error tolerance) were studied in Z mode using particle tracking. By optimizing twiss parameters and emittance of the injected beam, injection efficiency was substantially improved. For the particle tracking simulations mentioned, a newly developed Python package called Xsuite was used. Computationally expensive jobs with high number of particles and turns were performed on CERN's Batch Service based on HTCondor.

Contents

1	Introduction	3
2	Theoretical Background	4
2.1	Charged Particle in Electromagnetic Field	4
2.2	Hamiltonian in Frenet-Serret Reference Frame	4
2.3	Multipole Expansion of Magnetic Field	5
2.4	Equation of Motion	6
2.5	Transport Matrices	7
2.6	Synchrotron Radiation	8
2.6.1	Longitudinal Damping	8
2.6.2	Transverse Damping	9
3	FCC-ee Collider Top-Up Injection	10
3.1	On-axis and Off-axis Injection	10
3.2	Optics at the Injection Section	13
3.3	Thin Lattice and Tapering	14
3.4	Transverse and Longitudinal Damping Time	14
3.5	Transverse On-Momentum Dynamic Aperture	15
3.6	Transverse Off-Momentum Dynamic Aperture	16
3.7	Non-Linear Dispersion	18
3.7.1	Method	18
3.7.2	Results for the Lattice without Injection Optics	20
3.7.3	Results for the Lattice with Injection Optics	21
4	Hybrid On-Off Axis Injection	23
4.1	Hybrid Injection Scheme	23
4.2	Twiss Parameters of Injected Beam	23
4.3	Parameter Scan for Betatron and Momentum Offset	24
4.4	Scan for Injected Beam Vertical Emittance	25
5	Conclusion	27

1 Introduction

In the 2013 update of the European Strategy for Particle Physics, it was recommended that CERN undertake design studies for new high-energy frontier colliders, including proton-proton and electron-positron machines [4]. Consequently, the design studies for the Future Circular Collider (FCC) began in 2014. The FCC Conceptual Design Report (CDR) was subsequently published in January 2019 [1]. In the 2020 Update of the European Strategy for Particle Physics, it was emphasized that an electron-positron Higgs factory should be the highest-priority next collider [5]. In line with this priority, the FCC collaboration is now preparing the Feasibility Study Report, which is expected to be released by March 2025.

Table 1: FCC-ee collider parameters for the GHC lattice as of May 29, 2024 [10].

Operation Mode		Z	WW	$H(ZH)$	$t\bar{t}$
Beam energy	[GeV]	45.6	80	120	182.5
# Of IPs		4			
Circumference	[km]	90.658728			
Energy loss / turn	[GeV]	0.0390	0.369	1.86	9.94
Hor. emittance at collision ε_x	[nm]	0.7	2.16	0.66	1.51
Ver. emittance at collision ε_y	[pm]	1.9	2.0	1.0	1.36
Energy spread (SR/BS) σ_δ	[%]	0.039 / 0.110	0.069 / 0.105	0.102 / 0.176	0.152 / 0.184
Bunch length (SR/BS) σ_z	[mm]	5.57 / 15.6	3.46 / 5.28	3.26 / 5.59	1.91 / 2.32
Long. damping time	[turns]	1171	218	65.4	19.4
RF acceptance	[%]	1.06	3.32	2.06	3.06
Energy acceptance (DA)	[%]	± 1.0	± 1.0	± 1.9	-2.8/+2.5

The FCC-ee is designed to study the Z , W , H , and t particles with the highest precision [1]. Achieving this physics goal requires a significant increase in integrated luminosity compared to previous lepton colliders, but the very short beam lifetime poses a critical limitation [10]. To address this, top-up injection is necessary for the collider. This study investigates several key aspects of the FCC-ee top-up injection scheme through particle tracking.

The second part of this study provides the theoretical background used in particle tracking, including the equations of motion, transport matrix formalism, and synchrotron radiation. The third part details the collider's top-up injection scheme and presents results from various studies on the lattice with injection optics. In the fourth part, the hybrid on-off axis injection scheme is introduced and explained, along with the results of optimization studies for the Twiss parameters, betatron offset, momentum offset, and vertical emittance of the injected beam.

2 Theoretical Background

2.1 Charged Particle in Electromagnetic Field

The Lagrangian of a charged particle in electromagnetic field is given by:

$$L = -mc^2 \sqrt{1 - \frac{v^2}{c^2}} - e\Phi + e\vec{v} \cdot \vec{A} \quad (2.1)$$

where m is the mass, e is the charge, $\vec{v} = \frac{d\vec{r}}{dt}$ is the velocity and \vec{r} is the position of the particle respectively. Φ is the scalar potential and \vec{A} is the vector potential. These potentials are related to electric field \vec{E} and magnetic field \vec{B} by the following equations respectively:

$$\begin{aligned} \vec{E} &= -\vec{\nabla}\Phi - \frac{\partial \vec{A}}{\partial t} \\ \vec{B} &= \vec{\nabla} \times \vec{A} \end{aligned} \quad (2.2)$$

Equation of motion can be derived from the Euler-Lagrange equation 2.3.

$$\frac{d}{dt} \left(\frac{\partial L}{\partial \dot{q}_i} \right) - \frac{\partial L}{\partial q_i} = 0 \quad (2.3)$$

The Hamiltonian can be obtained by performing a Legendre transform on the Lagrangian:

$$H = c \sqrt{m^2 c^2 + \left(\vec{P} - e\vec{A} \right)^2} + e\Phi \quad (2.4)$$

where $\vec{P} = \vec{p} + e\vec{A}$ is the canonical momentum and \vec{p} is the mechanical momentum [7].

2.2 Hamiltonian in Frenet-Serret Reference Frame

Particle motion in an accelerator can be defined with respect to a reference orbit $\vec{r}_0(s)$:

$$\vec{r}(s) = \vec{r}_0(s) + \delta \vec{r}(s) \quad (2.5)$$

where arc-length parameter s is used to parameterise the curve. Motion around the reference orbit can be parameterised using the following unit vectors:

$$\begin{aligned} \hat{s}(s) &= \frac{d\vec{r}_0(s)}{ds} && : \text{Unit tangent vector} \\ \hat{x}(s) &= -\rho(s) \frac{d\hat{s}(s)}{ds} && : \text{Unit normal vector} \\ \hat{y}(s) &= \hat{s}(s) \times \hat{x}(s) && : \text{Unit bi-normal vector} \end{aligned} \quad (2.6)$$

where $\rho(s) = -\frac{1}{\left\| \frac{d\hat{s}(s)}{ds} \right\|}$ is the radius of curvature of the orbit. Using the orthonormal vectors given in equation 2.6, particles position around reference orbit can be expressed as:

$$\vec{r}(s) = \vec{r}_0(s) + x\hat{x}(s) + y\hat{y}(s) \quad (2.7)$$

To obtain the Hamiltonian in this reference frame, a canonical transformation of Hamiltonian 2.4 should be performed using the following generating function [7]:

$$F_3(P_i, \tilde{q}_i) = P_i \tilde{q}_i \quad (2.8)$$

where \sim denote variable in the new coordinates (x, y, s) as given in equations 2.6. Assuming a planer motion and changing the independent variable from t to s , one obtains the Hamiltonian [7]:

$$\tilde{H} = - \left(1 + \frac{x}{\rho}\right) \left[\left(\frac{H - e\Phi}{c} \right)^2 - m^2 c^2 - (P_x - eA_x)^2 - (P_y - eA_y)^2 \right]^{1/2} - eA_s \quad (2.9)$$

Expanding the Hamiltonian up to second order in P_x and P_y gives [7]:

$$\tilde{H} \simeq -P \left(1 + \frac{x}{\rho}\right) + \frac{1 + x/\rho}{2P} [(P_x - eA_x)^2 + (P_y - eA_y)^2] - eA_s \quad (2.10)$$

where $P = \sqrt{(E^2/c^2 - m^2 c^2)^2}$ and $E = H - e\phi$.

2.3 Multipole Expansion of Magnetic Field

In a region with no charges and no electric field, Maxwell's equations for magnetic field \vec{B} reduce to following equations:

$$\begin{aligned} \nabla \cdot \vec{B} &= 0 \\ \nabla \times \vec{B} &= 0 \end{aligned} \quad (2.11)$$

Second of those equations implies that magnetic field \vec{B} is a conservative field. Therefore it can be written as the gradient of a scalar function f , that is:

$$\vec{B} = \nabla f \quad (2.12)$$

Plugging this into the first of equations 2.11 gives Laplace equation for the potential f :

$$\nabla^2 f = 0 \quad (2.13)$$

Assuming magnetic field doesn't change in the s direction, this equation has the following solution on $x - y$ plane in polar coordinates (r, φ) :

$$f = \sum_{n=1}^{\infty} A_n r^n \sin(n(\varphi - \alpha_n)) \quad (2.14)$$

where A_n and α_n are some constant. Taking the gradient of f one obtains the radial and polar components of the magnetic field. It can be shown that the horizontal and vertical components of the magnetic field \vec{B} is given by:

$$\begin{aligned}
B_x(r, \varphi) &= \sum_{n=1}^{\infty} A_n n r^{n-1} \sin((n-1)\varphi - n\alpha_n) \\
B_y(r, \varphi) &= \sum_{n=1}^{\infty} A_n n r^{n-1} \cos((n-1)\varphi - n\alpha_n)
\end{aligned} \tag{2.15}$$

These two components of magnetic field can be combined in one complex quantity.

$$\begin{aligned}
B_y + iB_x &= \sum_{n=1}^{\infty} A_n n r^{n-1} e^{i((n-1)\varphi - n\alpha_n)} \\
&= B_0 \sum_{n=0}^{\infty} (b_n + ia_n) \left(\frac{x + iy}{r_0} \right)^n
\end{aligned} \tag{2.16}$$

where $z = x + iy = re^{i\varphi}$. In this expansion, a_n is called skew component and b_n is called normal component. For $n = 0$ one gets the dipole component, for $n = 1$ the quadrupole component, for $n = 2$ the sextupole and so on. These multipole coefficients are determined by the following equations:

$$\begin{aligned}
a_n &= \frac{r_0^n}{B_0 n!} \left. \frac{\partial^n B_x}{\partial x^n} \right|_{x=y=0} \\
b_n &= \frac{r_0^n}{B_0 n!} \left. \frac{\partial^n B_y}{\partial x^n} \right|_{x=y=0}
\end{aligned} \tag{2.17}$$

2.4 Equation of Motion

By applying Hamilton's equations to Eq. 2.10 and neglecting synchrotron motion, the equations of motion in the transverse plane are obtained as:

$$\begin{aligned}
x'' &= \frac{1}{\rho} \left(1 + \frac{x}{\rho} \right) + \frac{B_y}{B_0 \rho} \frac{p_0}{p} \left(1 + \frac{x}{\rho} \right)^2 \\
y'' &= -\frac{B_x}{B_0 \rho} \frac{p_0}{p} \left(1 + \frac{x}{\rho} \right)^2
\end{aligned} \tag{2.18}$$

where the particle charge was replaced by $p_0/B_0\rho$ [7]. The quantity $B_0\rho$ is called the beam rigidity and it is given by the following equation:

$$B_0\rho = \frac{p_0}{q} \tag{2.19}$$

Considering only the dipole and quadrupole components of the multipole expansion given by Eq. 2.16, one obtains the following magnetic field components:

$$\begin{aligned} B_x &= Gy \\ B_y &= -B_0 + Gx \end{aligned} \quad (2.20)$$

where $G = \frac{\partial B_x}{\partial y} = \frac{\partial B_y}{\partial x}$ is the quadrupole gradient. Plugging these magnetic fields on the equations of motion for transverse plane and taking $p = p_0 + \delta p_0$ with δ small and assuming $x \ll \rho$ gives:

$$\begin{aligned} x'' + \left(\frac{1}{\rho(s)^2} - k(s) \right) x &= \frac{\delta}{\rho} \\ y'' + k(s)y &= 0 \end{aligned} \quad (2.21)$$

where the normalized quadrupole coefficient was defined as $k(s) = \frac{G}{B_0 \rho}$ [7]. Eq. 2.21 is called Hill's equation.

2.5 Transport Matrices

The linearized equation of motion for betatron motion is given by Hill's equation [7]:

$$x'' + K(s)x = 0 \quad (2.22)$$

$K(s)$ is called the focusing function and it is piece-wise continuous for an accelerator. Solutions to this equation with $K = k_0(const.)$ is given by:

$$x(s) = \begin{cases} c_1 \cos(\sqrt{k_0}s) + c_2 \sin(\sqrt{k_0}s) & \text{if } k_0 > 0 \\ c_1 x + c_2 & \text{if } k_0 = 0 \\ c_1 \cosh(\sqrt{|k_0|}s) + c_2 \sinh(\sqrt{|k_0|}s) & \text{if } k_0 < 0 \end{cases} \quad (2.23)$$

To apply the transfer matrix formalism, the betatron state vector $\vec{x}(s)$ is defined as follows:

$$\vec{x}(s) = \begin{bmatrix} x(s) \\ x'(s) \end{bmatrix} \quad (2.24)$$

The solution can then be expressed in terms of the betatron transfer matrix M :

$$\vec{x}(s) = M(s|s_0)\vec{x}(s_0) \quad (2.25)$$

The betatron transfer matrix $M(k_0, L)_{QF}$ of a focusing quadrupole of length L and strength k_0 is given by [7]:

$$M(k_0, L)_{QF} = \begin{bmatrix} \cos(\sqrt{k_0}L) & \frac{1}{\sqrt{k_0}} \sin(\sqrt{k_0}L) \\ -\sqrt{k_0} \sin(\sqrt{k_0}L) & \cos(\sqrt{k_0}L) \end{bmatrix} \quad (2.26)$$

Similarly the betatron transfer matrix $M(k_0, L)_{QD}$ of a defocusing quadrupole of length L and strength k_0 is given by [7]:

$$M(k_0, L)_{QD} = \begin{bmatrix} \cosh(\sqrt{|k_0|}L) & \frac{1}{\sqrt{|k_0|}} \sinh(\sqrt{|k_0|}L) \\ -\sqrt{|k_0|} \sinh(\sqrt{|k_0|}L) & \cosh(\sqrt{|k_0|}L) \end{bmatrix} \quad (2.27)$$

Finally the transfer matrix of a drift of length L is given by [7]:

$$M(L)_{Drift} = \begin{bmatrix} 1 & L \\ 0 & 1 \end{bmatrix} \quad (2.28)$$

To get the transfer matrix for a line of n number of elements, transfer matrix of each elements needs to be multiplied:

$$M_{tot} = M_n M_{n-1} M_{n-2} \dots M_3 M_2 M_1 \quad (2.29)$$

2.6 Synchrotron Radiation

Average synchrotron radiation power of an electron over one turn $\langle P_\gamma \rangle$ is given by the follow the following equation [11]:

$$\langle P_\gamma \rangle = \frac{c}{2\pi} C_\gamma E^4 \left\langle \frac{1}{\rho^2} \right\rangle = C_\gamma E^4 \frac{f_{rev}}{2\pi} \oint \frac{ds}{\rho^2} \quad (2.30)$$

where c is the speed of light in vacuum, E is the total energy of the particle ρ is the bending radius, f_{rev} is the revolution frequency and C_γ is the Sand's radiation constant and given by the following equation [11]:

$$C_\gamma = \frac{4\pi}{3} \frac{r_c}{(mc^2)^3} = 8.8460 \times 10^{-5} \frac{\text{m}}{\text{GeV}^3} \quad (2.31)$$

where r_c is the classical radius of the particle given by $r_c = \frac{q^2}{4\pi\epsilon_0 mc^2}$, q is the charge of the particle, ϵ_0 is the permittivity of free space, and m is the mass of the particle.

2.6.1 Longitudinal Damping

Equation of motion for synchrotron oscillations is given by the following differential equation [11]:

$$\frac{d^2\varepsilon}{dt^2} + 2\alpha_s \frac{d\varepsilon}{dt} + \Omega^2 \varepsilon = 0 \quad (2.32)$$

where $\varepsilon = E - E_0$ is the energy offset with respect to synchronous particle energy E_0 , α_s is the damping constant and Ω is the synchrotron oscillation frequency. Longitudinal damping constant and synchrotron oscillation frequency is given by the following equations [11]:

$$\alpha_s = J_s \frac{\langle P_\gamma \rangle}{E_0} \quad (2.33)$$

$$\Omega^2 = \omega_0^2 \frac{h(\gamma^{-2} - \alpha_c) e V_{rf} \cos(\psi_s)}{2\pi E_0} \quad (2.34)$$

where $J_s = 2 + \vartheta$ is the synchrotron partition number, ω_0 is the angular revolution frequency, h is the integer harmonic number, γ is the relativistic gamma factor, e is the electron charge, V_{rf} is the peak cavity voltage, ψ_s is the synchronous phase and α_c is the momentum compaction factor. The correction on the synchrotron partition number is given by the following equation [11] :

$$\vartheta = \frac{\oint \frac{\eta}{\rho^3} (1 + 2k\rho^2) ds}{\oint \frac{1}{\rho^2} ds} \quad (2.35)$$

where η is the periodic dispersion function and k is the quadrupole strength function. The differential equation of motion for synchrotron oscillations 2.32 is same as the differential equation of a damped harmonic oscillator. The solution of this equation is [11]:

$$\varepsilon(t) = \varepsilon_0 e^{-\alpha_s t} \cos(\Omega t) \quad (2.36)$$

The amplitude of the energy offset is exponentially decreasing with the longitudinal damping time $\tau_s = 1/\alpha_s$.

2.6.2 Transverse Damping

Similarly to longitudinal damping, horizontal damping constant is given by [11]:

$$\alpha_x = J_x \frac{\langle P_\gamma \rangle}{E_0} \quad (2.37)$$

where $J_x = 1 - \vartheta$ is the horizontal partition number with ϑ defined in Eq. 2.35. Vertical damping constant is similar to vertical one and given by [11]:

$$\alpha_y = J_y \frac{\langle P_\gamma \rangle}{E_0} \quad (2.38)$$

where $J_y = 1$ is the vertical partition for a planer machine without any vertical bends. Horizontal and vertical times are defined as $\tau_x = 1/\alpha_x$ and $\tau_y = 1/\alpha_y$, respectively. Additionally, sum of the three damping times is a constant, that is:

$$J_x + J_y + J_s = 4 \quad (2.39)$$

3 FCC-ee Collider Top-Up Injection

As discussed in the FCC Conceptual Design Report, the decrease in beam current due to processes such as scattering and collisions needs to be compensated to maximize luminosity [1]. Top-up injection is the technique developed specifically for this purpose. As the name suggests, in the top-up injection, the beam is injected on top of the circulating beam to compensate for the previously mentioned losses. Charge accumulation in the collider during an operation with top-up injection is presented on the Fig. 1. As shown in the figure, the accumulated charge in the collider decreases over time until new particles are injected on top of the circulating beam. With top-up injection, charge accumulation can be balanced around the nominal value by periodically changing the type of injected particles with a correctly arranged frequency [9]. This technique requires a full-energy booster located in the collider tunnel. Top-up injection has been adopted by lepton accelerator facilities around the world, including light sources and colliders such as APS-U, SuperKEKB [8]. The conventional injection concept, which consists of two kicker magnets and a septum, is employed in the current scheme. There are two different injection schemes to create the transverse separation between the circulating and injected beams at the injection point where the septum blade is placed: on-axis injection and off-axis injection.

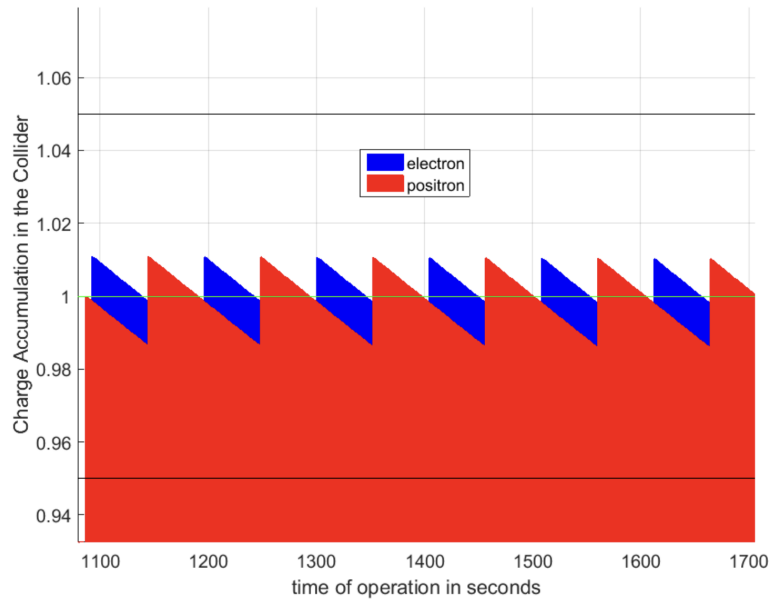


Figure 1: Beam current vs operation time with top-up injection [9]

3.1 On-axis and Off-axis Injection

On-axis and off-axis injection are the two schemes in which the transverse separation between the circulating and injected beams is achieved using different methods. In on-axis (synchrotron) injection, the injected beam has a momentum offset relative to the circulating beam and is injected into the dispersive closed orbit corresponding to that momentum offset. The injected beam then undergoes longitudinal synchrotron oscillations and eventually

damps into the circulating beam due to synchrotron radiation. In off-axis (betatron) injection, the beam is injected at the same energy as the circulating beam, but with a horizontal transverse separation. In this case, the beam performs transverse betatron oscillations and eventually damps into the circulating beam. Those two injection schemes are presented on Fig. 2 schematically.

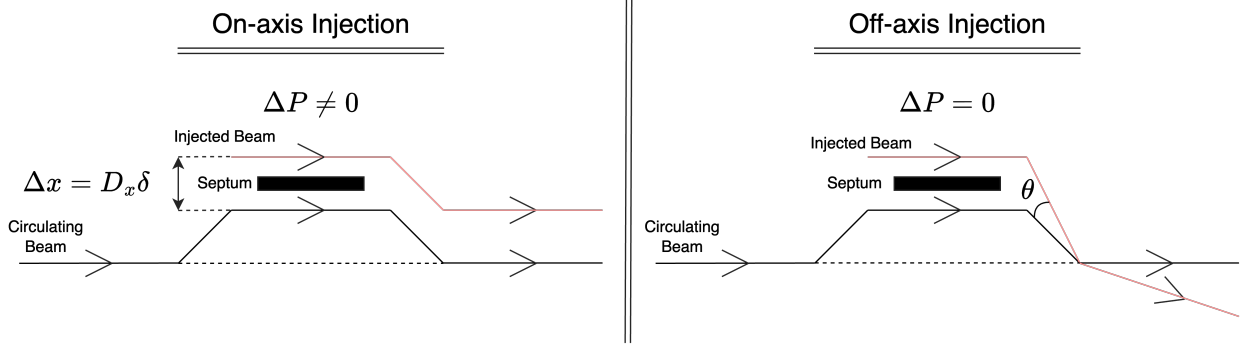


Figure 2: Schematic view of on-axis and off-axis injection

Both on-axis and off-axis injection were used in LEP [3]. During operation, on-axis injection became the preferred scheme due to several advantages over off-axis injection. One advantage is that, because of the shorter damping time in the longitudinal plane compared to the transverse plane, the injected beam damps into the circulating beam more quickly. Another advantage is that, since the transverse separation in on-axis injection is due to dispersion at the injection point, the injected beam follows the same trajectory as the circulating beam in the low-dispersion straight section. This results in higher injection efficiency and lower radiation doses to the experiments. Finally, on-axis injection was also found to be more robust against injection errors compared to off-axis injection [2]. Given the advantages of on-axis injection and the infeasibility of off-axis injection [12], on-axis injection has been chosen as the baseline scheme for the FCC-ee collider top-up injection.

For the on-axis injection of the FCC-ee collider, clearances from the injection septa were chosen to be 5σ [1]. A schematic diagram of the transverse real space at the injection point can be seen in Fig. 3.

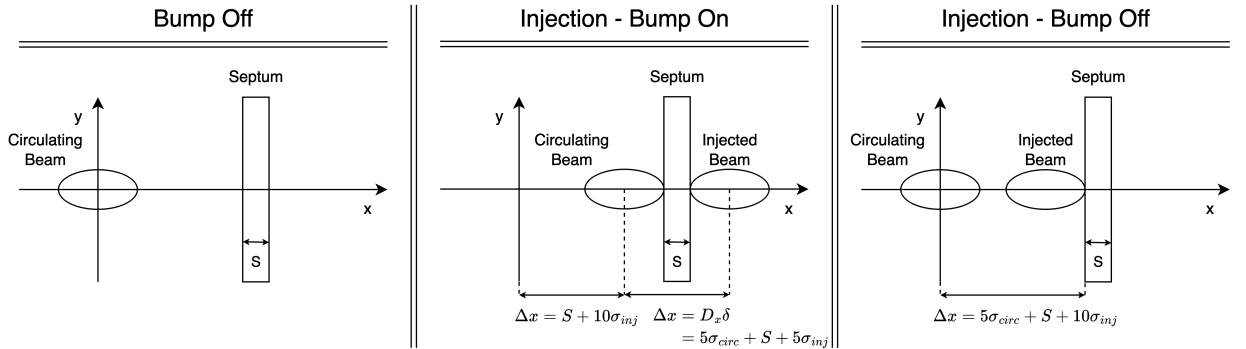


Figure 3: Transverse real space diagrams at injection point with 5σ beam envelopes

From Fig. 3, three requirements for on-axis injection can be inferred. The first requirement is beam separation. At the injection point, the horizontal separation between the circulating beam and the injected beam is given by $5\sigma_{circ} + S + 5\sigma_{inj}$, which should be equal to $|D_x\delta_{offset}|$ for a pure on-axis injection. The second requirement involves the septum position: after the bump turns off, the septum should be positioned far enough from the injected beam. Therefore, the position of the septum should be equal to $5\sigma_{circ} + S + 10\sigma_{inj}$. Finally, the bump height can be directly obtained from the geometry as $S + 10\sigma_{inj}$. The three described requirements are mathematically expressed in the following equations:

$$|D_x\delta_{offset}| = 5\sigma_{circ} + S + 5\sigma_{inj} \quad (3.1)$$

$$x_{septa} = 5\sigma_{circ} + S + 10\sigma_{inj} \quad (3.2)$$

$$\Delta x_{bump} = S + 10\sigma_{inj} \quad (3.3)$$

where

- S : septum thickness
- D_x : horizontal dispersion at the injection point
- δ_{offset} : momentum offset of the injected beam
- Δx_{bump} : bump height
- x_{septa} : septum position
- σ_{circ} : RMS beam envelope of circulating beam
- σ_{inj} : RMS beam envelope of injected beam

RMS beam envelopes at the injection point are given by the following equations:

$$\sigma_{circ} = \sqrt{\beta_x \epsilon_x + (D_x \sigma_\delta^{circ})^2} \quad (3.4)$$

$$\sigma_{inj} = \sqrt{\beta_x^{inj} \epsilon_x^{inj} + (D_x^{inj} \sigma_\delta^{inj})^2} \quad (3.5)$$

- β_x : horizontal beta function at injection point
- ϵ_x : horizontal geometric emittance of the circulating beam
- σ_δ^{circ} : RMS momentum spread of circulating beam
- β_x^{inj} : horizontal beta function of injected beam
- ϵ_x^{inj} : horizontal geometric emittance of the injected beam
- D_x^{inj} : horizontal dispersion of injected beam at the injection point
- σ_δ^{inj} : RMS momentum spread of injected beam

3.2 Optics at the Injection Section

To ensure the requirements for the on-axis injection given in Eqs. 3.1 - 3.2 a special optics design was previously developed [12]. In this study, 5σ beam envelopes of both the injected beam and the circulating beam were generated with Xsuite [6]. The calculated twiss parameters are shown in Fig. 4 and 5σ beam envelopes can be seen in Fig. 5. With the new injection optics, horizontal dispersion of -1.6 m which is necessary for on-axis injection was achieved at the injection point and horizontal beta function at the injection point was increased to 1014 m.

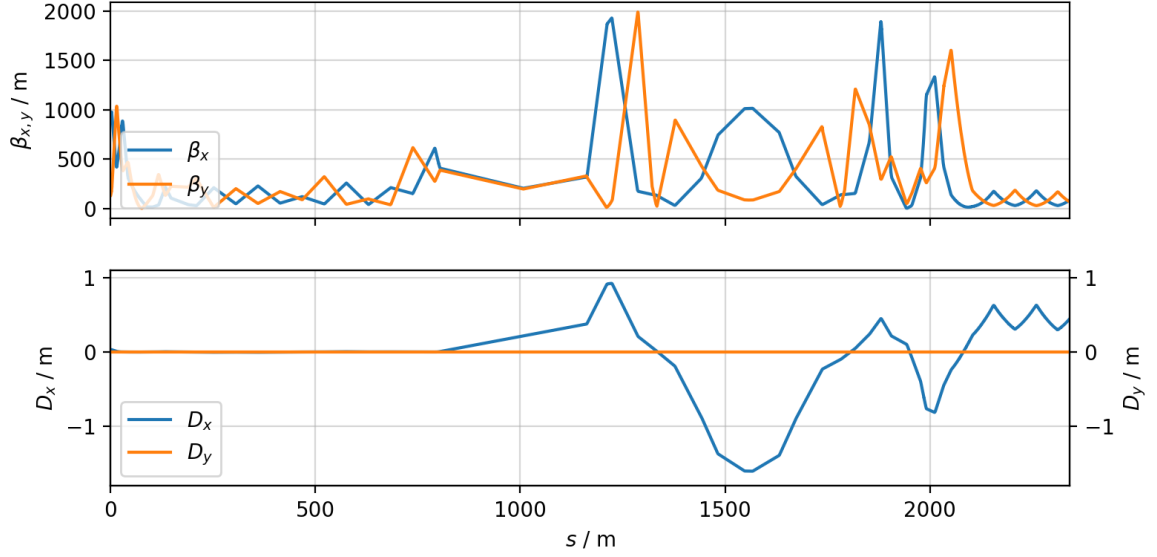


Figure 4: Twiss parameters at injection section

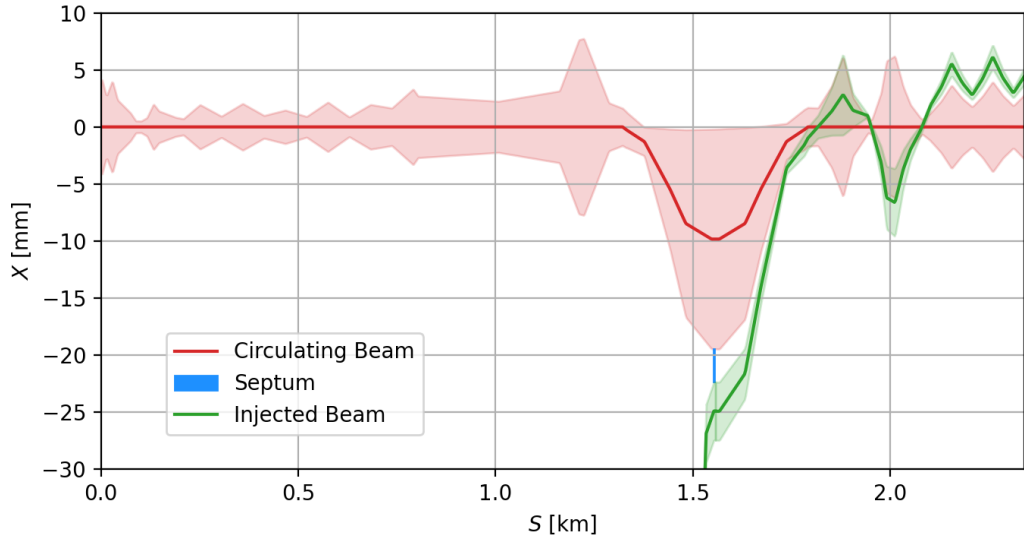


Figure 5: 5σ Beam envelopes in the injection section - bump on

To check if the changes in the optics at the injection section introduced any unexpected variations in the collider parameters (such as transverse and longitudinal damping times, on-off momentum dynamic aperture), several tests were performed using particle tracking.

3.3 Thin Lattice and Tapering

Particle tracking with synchrotron radiation in Xsuite is only compatible with lattices composed of thin elements. Therefore, both the original lattice and the lattice with injection optics were thinned using MadX, with 20 slices per element, except for the final focusing magnets and RF cavities, which were sliced into 50 and 1 slice, respectively. Additionally, both lattices were tapered and the local momentum offset was set to zero at the middle of the RF section. The local momentum offset deviation with respect to the position on the collider ring at the Z mode is presented on the Fig. 6. It can also be seen on the same figure that the momentum offset reduces at arc sections, keeps constant at the straight sections and increases at the RF section. Additionally, it is clear that the momentum offset is nonzero in the injection straight section. Therefore, this momentum deviation should be accounted for in the design of the injection optics. The energy loss per turn was found to be 39.1 MeV, which is in good agreement with the value given in the parameter table 1.

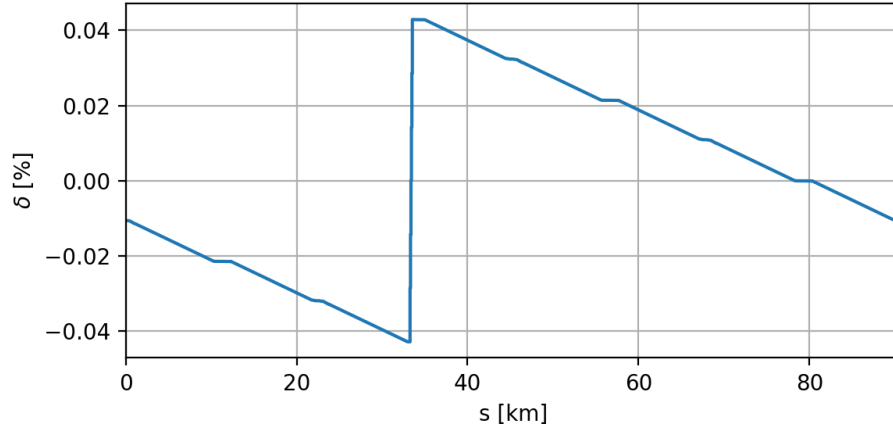


Figure 6: Local momentum offset vs position on the collider ring

3.4 Transverse and Longitudinal Damping Time

To evaluate the effect of injection optics on transverse and longitudinal damping times using particle tracking, three particles were tracked on both the original lattice and the lattice with injection optics. One of the particles served as the reference particle for control, while the other two particles were given small transverse and momentum offsets relative to the reference particle to assess transverse and longitudinal damping, respectively. The particles were tracked on the corresponding lattices for 5000 turns starting from the injection point. Their 6D coordinates were recorded by a particle monitor at each turn. An exponential fit was applied to the transverse amplitude and momentum offset of the corresponding particles. The tracking results with the applied exponential fits can be seen in Fig. 7.

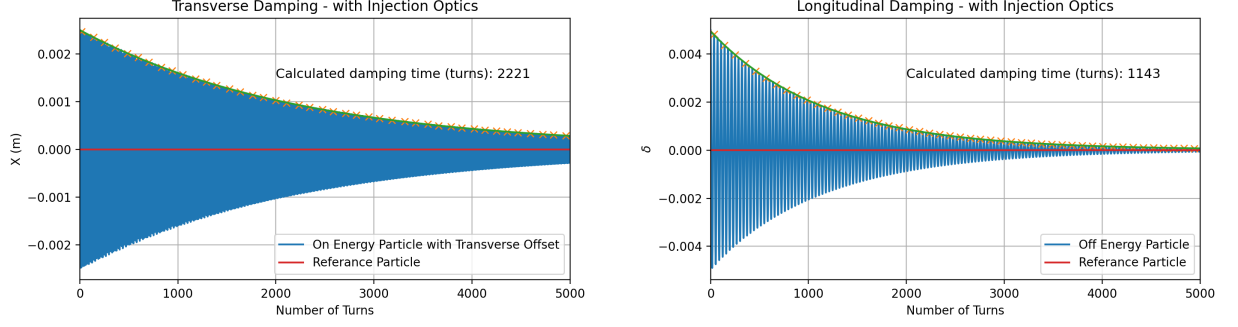


Figure 7: Transverse and longitudinal damping of particles on the lattice with injection optics.

The damping times computed by two different methods —tracking and Xsuite Twiss—are presented in Table 2. No differences were observed in the damping times calculated by Xsuite Twiss, while the tracking method showed a variation of approximately $\pm 5.7\%$ in the transverse damping time and $\pm 2.6\%$ in the longitudinal damping time. The maximum discrepancy between the two methods was found to be around $\pm 5\%$. These results were considered acceptable for the rest of the study.

Table 2: Found damping times (number of turns)

	without injection optics		with injection optics	
	transverse	longitudinal	transverse	longitudinal
computed by tracking	2355	1174	2221	1143
computed by Xsuite twiss	2333	1166	2333	1166

3.5 Transverse On-Momentum Dynamic Aperture

The transverse on-momentum dynamic aperture of the collider lattice, with and without injection optics, was studied using particle tracking. In this study, a polar grid of particles was created in the first quadrant of the normalized X-Y plane. The particles were then tracked for 800 turns starting from the injection point. The results can be seen in Fig. 8. No significant effect of the injection optics was observed.

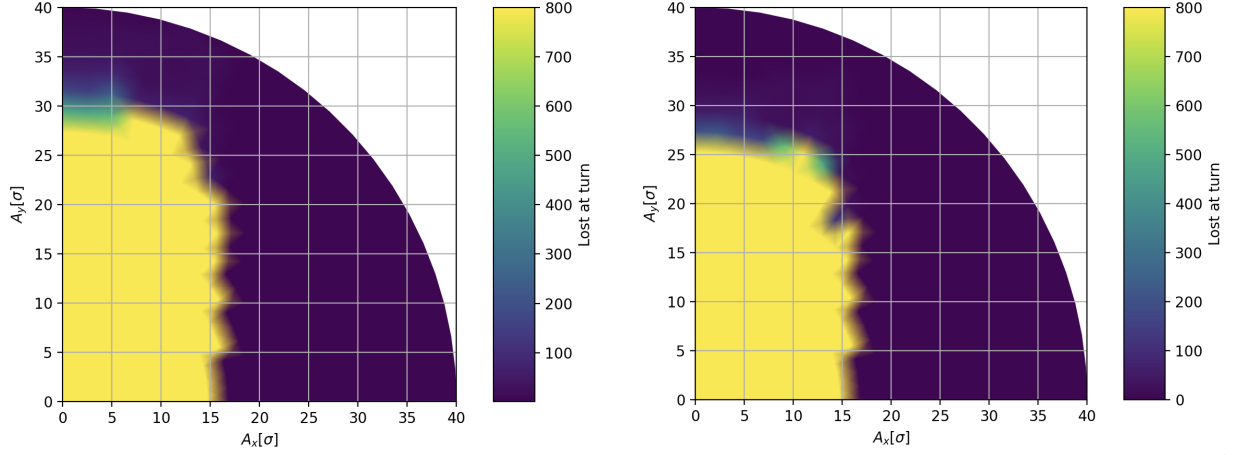


Figure 8: Transverse on-momentum dynamic aperture of the lattice with and without injection optics

3.6 Transverse Off-Momentum Dynamic Aperture

A 5σ transverse off-momentum dynamic aperture at $\delta = \pm 1.0\%$ is needed for pure on-axis injection. Therefore, the transverse off-momentum dynamic aperture of the collider lattice, with and without injection optics, was studied using particle tracking. In this study, a polar grid of particles corresponding to same normalized amplitudes, with energy offset values between $\pm 1.1\%$, was first created at the injection point. An example of such a particle distribution is shown in Fig. 9. These particles were then tracked on the lattice, with and without injection optics, for 3000 turns. The tracking results are presented in Fig. 10 and Fig. 11. In these figures ϕ stands for the angle of particle distribution in the normalized phase space.

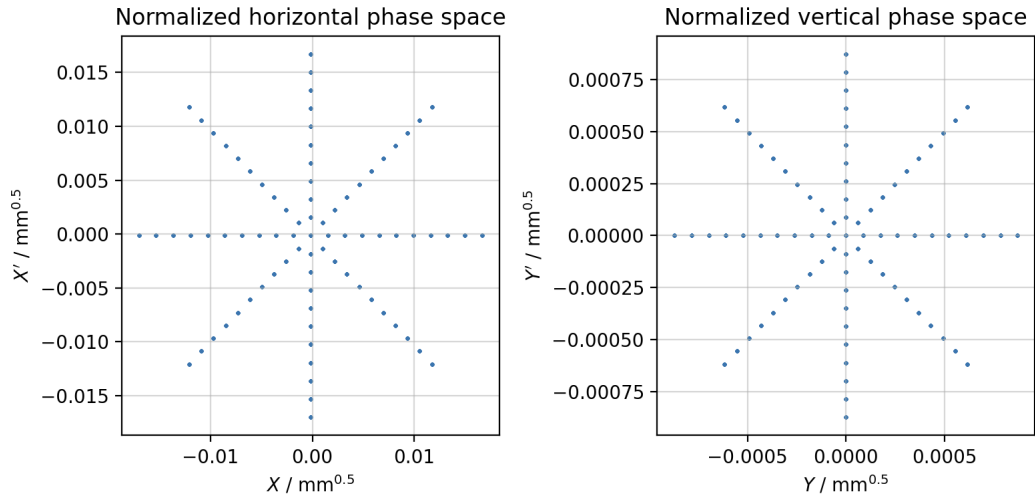


Figure 9: Grid of particles in the transverse phase space

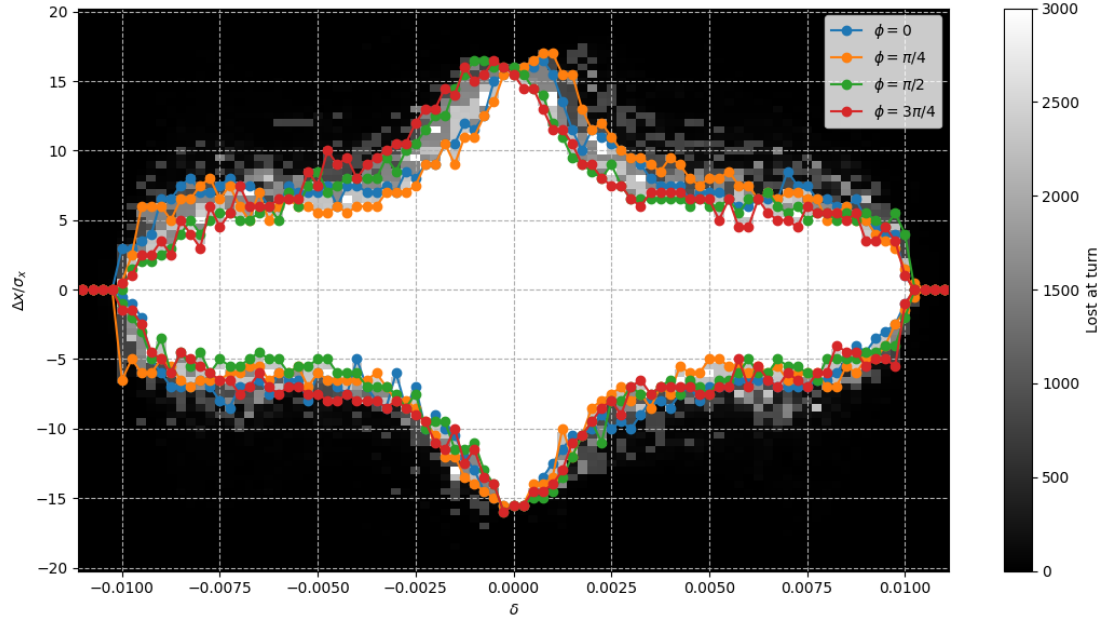


Figure 10: Momentum acceptance of the lattice without injection optics

As shown in Fig. 11, a significant reduction in the transverse off-momentum dynamic aperture was observed after introducing the injection optics to the original lattice. For pure on-axis injection with the previously designed injection optics, a 5σ aperture is required at a momentum offset of $\delta = \pm 1.0\%$. However, with the injection optics, only a $\sim 3\sigma$ aperture was achieved at $\delta = \pm 0.5\%$. Consequently, the rest of the study focused on implementing and assessing the feasibility of a hybrid on-off axis injection scheme.

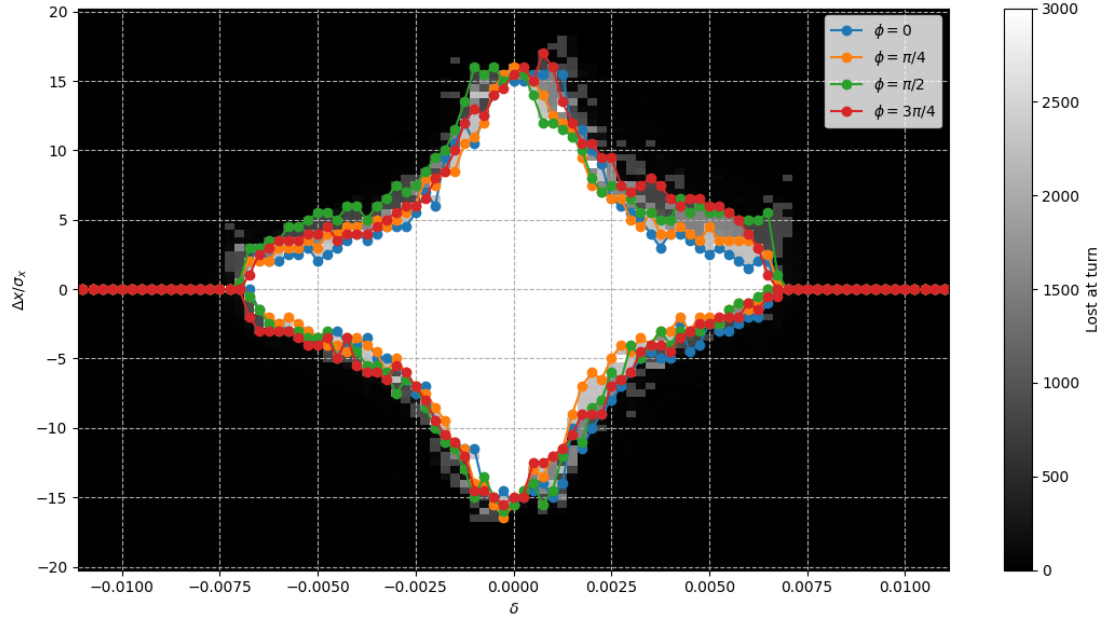


Figure 11: Momentum acceptance of the lattice with injection optics

3.7 Non-Linear Dispersion

3.7.1 Method

To achieve purely on axis injection, non-linear dispersion at high momentum offsets needs to be studied. For this purpose a new analysis method was developed. In this method, a grid of particles corresponding to each value of momentum offset is created in the horizontal phase space around the point predicted by the second-order dispersion, which serves as an initial guess. An example of such a grid of particles is presented on Fig. 12.

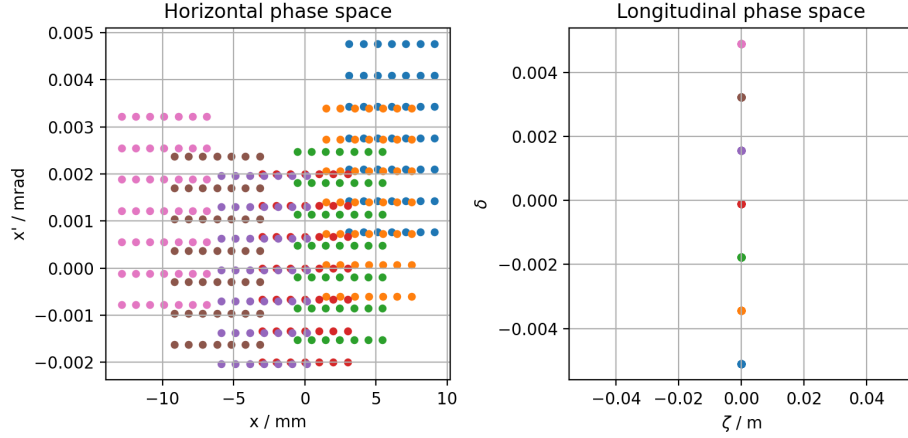


Figure 12: An example of a particle distribution used in non-linear dispersion study. Each color corresponds to a unique momentum offset.

These particles were then tracked on the considered lattice for 800 turns, starting at the injection point. Using a particle monitor, the 6D positions of the particles were recorded at the same point. The X position of each particle, corresponding to same momentum offset, was then plotted. A filter created by taking the Fourier transform of the data was applied on each plot to filter out high frequencies that increase the horizontal amplitude.

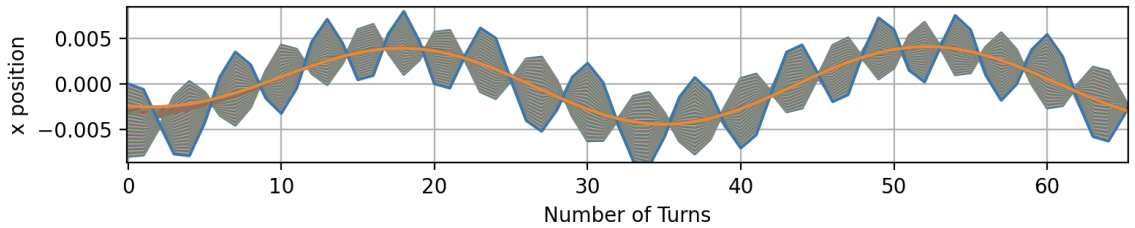


Figure 13: X position (in meters) of each particle at each turn

A relative error for each particle was calculated based on the low-frequency signal. The calculated errors were then plotted on a 2D density plot, as shown in Fig. 14. The minimum point of the plot was identified and considered as the closed orbit. The points corresponding to the lowest relative error for each value of momentum offset were plotted alongside the

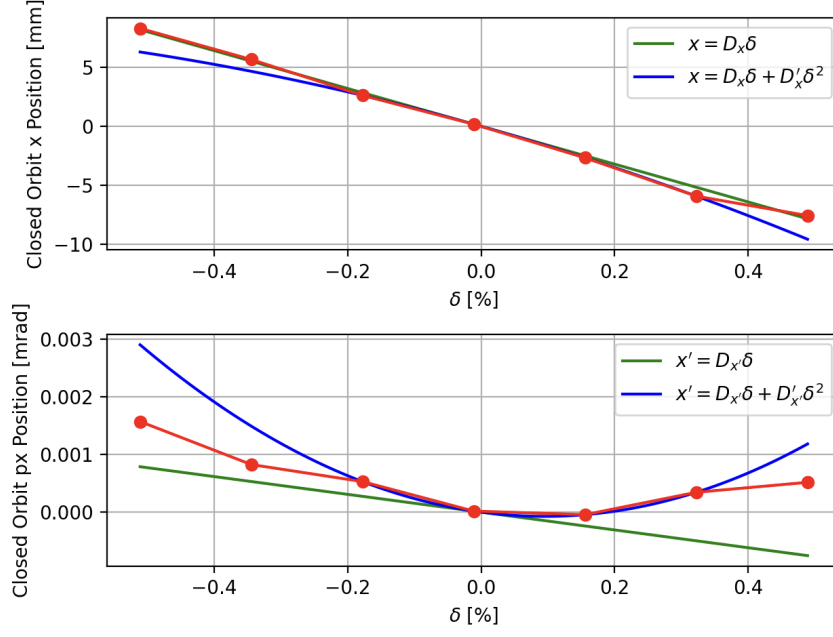


Figure 15: Found closed orbit positions (shown with red dots) vs momentum offset

first and second-order dispersion curves calculated using the Twiss method in Xsuite for comparison.

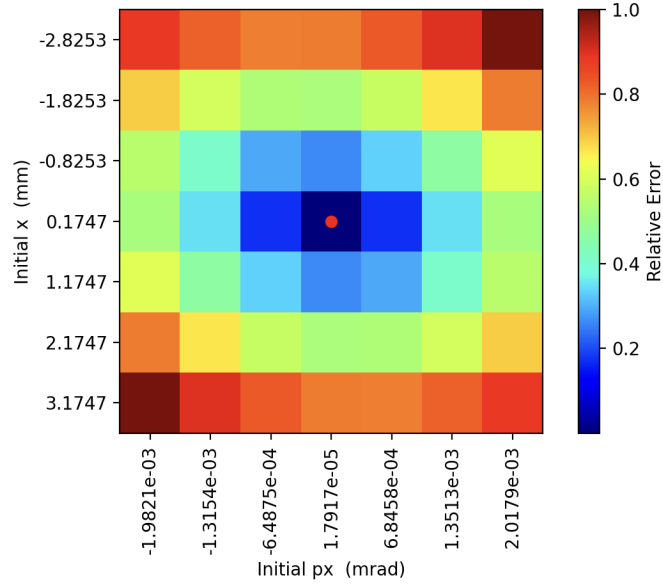


Figure 14: Relative error density plot of a grid of initial x and px values for a single momentum offset

The same method was applied using a much finer grid of particles around the second-order dispersion as an initial guess for both lattices with and without injection optics.

3.7.2 Results for the Lattice without Injection Optics

The results obtained for the lattice without injection optics agree well with the second-order dispersion, as shown in Fig. 17.

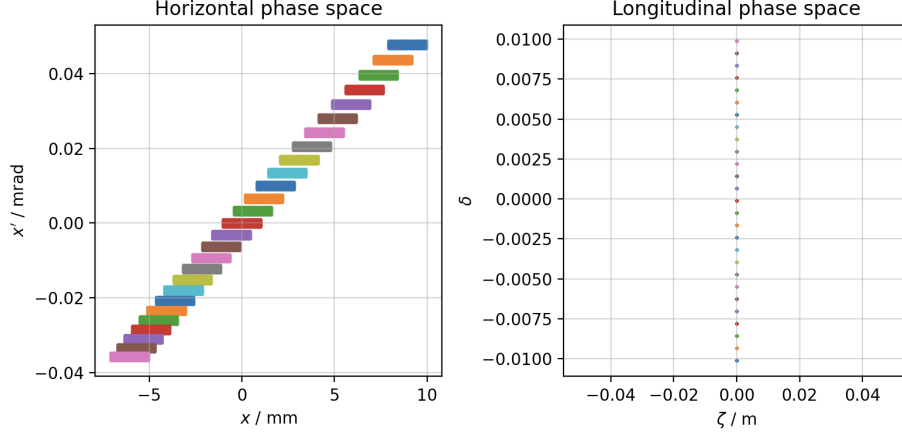


Figure 16: Initial grid of particles used in non-linear dispersion study of the lattice without injection optics. Colors represent corresponding momentum offsets.

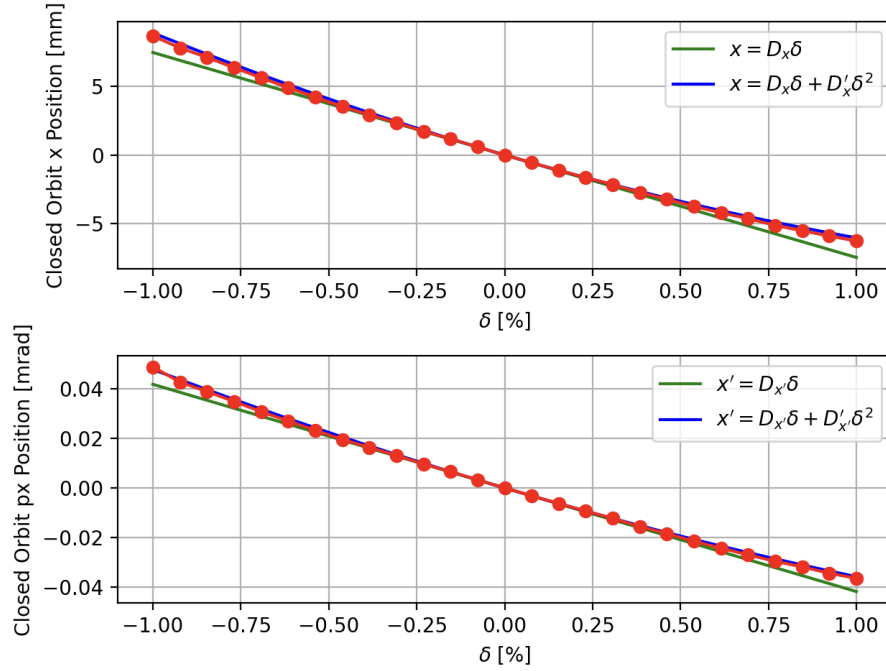


Figure 17: Found closed orbit positions for various momentum offset values on the lattice without injection optics

3.7.3 Results for the Lattice with Injection Optics

The results obtained for the lattice with injection optics don't agree well with the second-order dispersion as the lattice without injection optics, as shown in Fig. 19. Higher-order effects were observed to have an increasingly significant impact as the momentum offset increased.

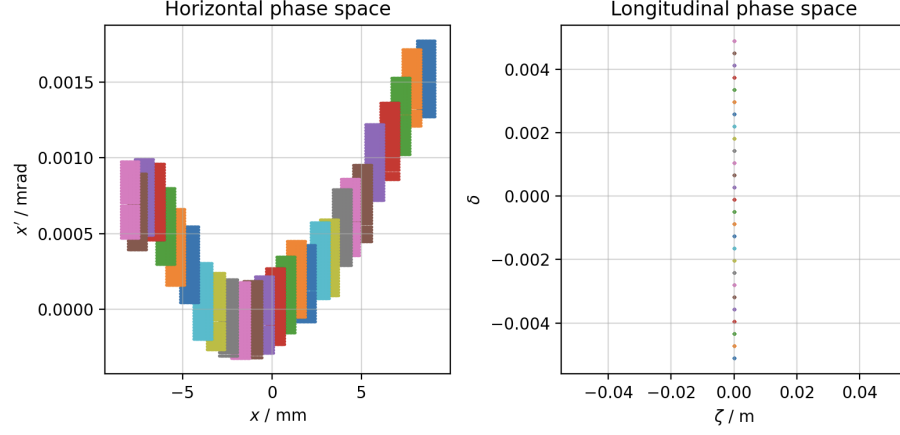


Figure 18: Initial grid of particles used in non-linear dispersion study of the lattice with injection optics. Colors represent corresponding momentum offsets.

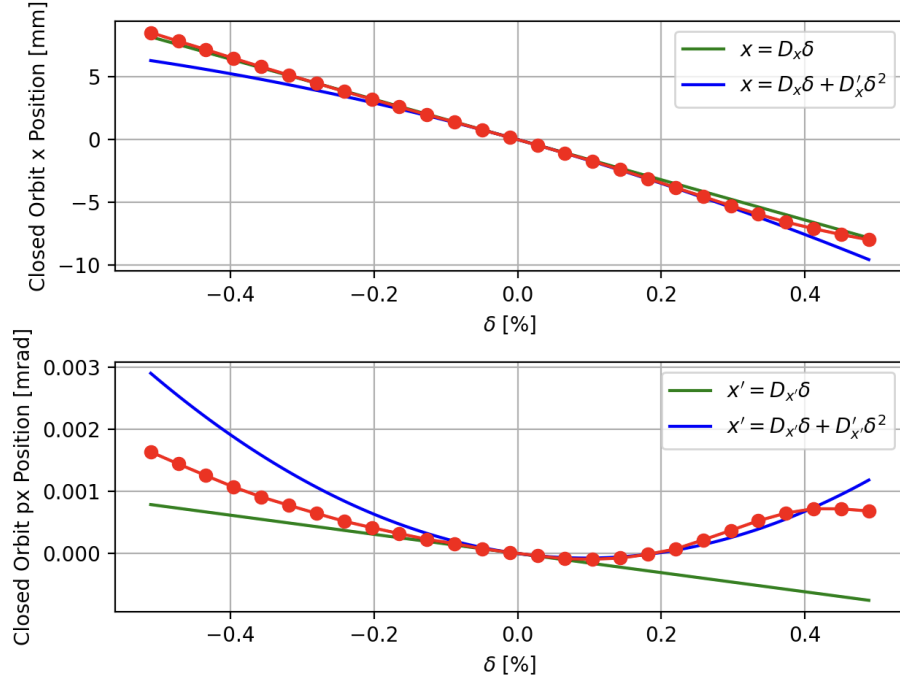
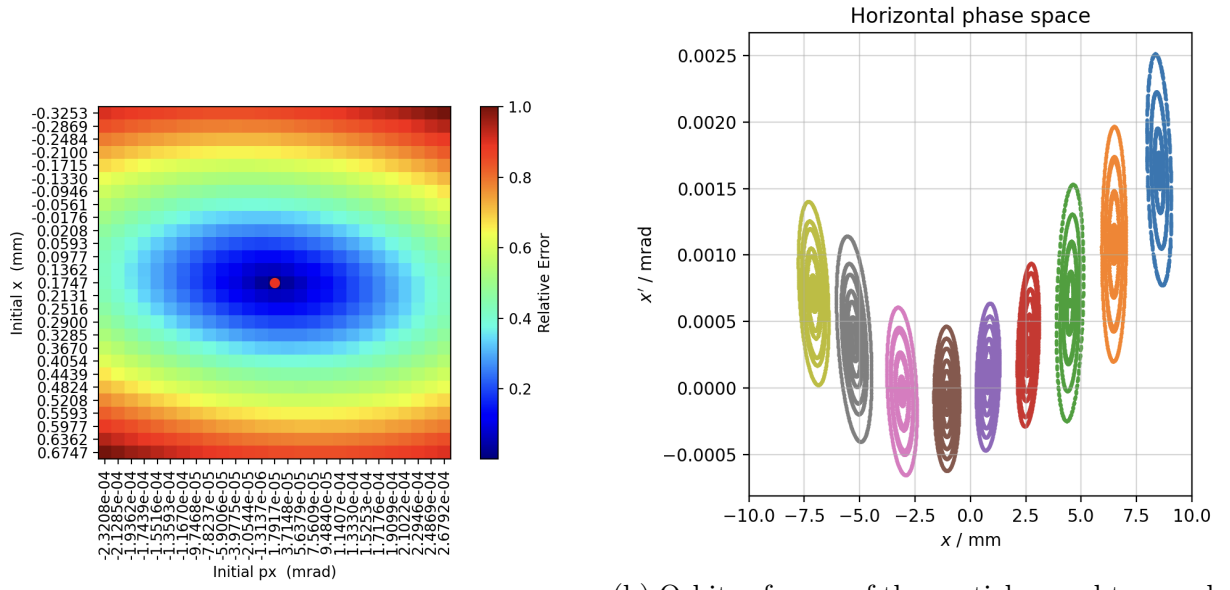


Figure 19: Found closed orbit positions for various momentum offset values on the lattice with injection optics



(a) Relative error density plot of a fine grid of initial x and p_x values for a single momentum offset

(b) Orbits of some of the particles used to search closed orbit on the lattice with injection optics. They are grouped with their momentum offsets in colors.

Figure 20: An example of a non-linear dispersion study on a fine grid of particles.

4 Hybrid On-Off Axis Injection

4.1 Hybrid Injection Scheme

Given the reduction in the transverse off-momentum dynamic aperture (see Sec. 3.6), the feasibility of hybrid on-off axis injection was investigated by particle tracking. In hybrid injection scheme injected beam has a momentum offset as well as a betatron offset with respect to the corresponding closed orbit. As an example, with $D_x = -1.6$ m and $\delta_{offset} = 0.5\%$ closed orbit position becomes $x = -8$ mm. In order to achieve 2.8 mm separation between 5σ beam envelopes of injected and circulating beam, injected beam should be given 1.8 mm betatron offset. This scheme is presented on Fig. 21.

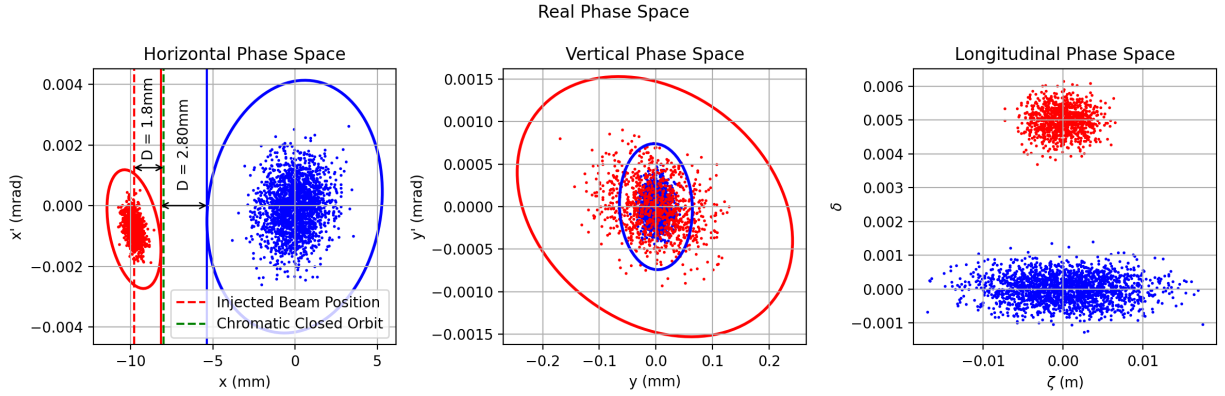


Figure 21: Real phase space of injected (red) and circulating (blue) beam. On the horizontal phase space plot 2.80 mm septa separation between 5σ beam envelopes and 1.8 mm betatron offset is shown.

4.2 Twiss Parameters of Injected Beam

During the initial parameter scans for hybrid injection, on-momentum twiss parameters were used for injected beam. In some of the tracking results a filamentation in the vertical phase space was observed. An example of one of the observed filamentations is presented on Fig. 22. This filamentation was found to be due to the vertical mismatch of the injected beam. Additionally, the unsymmetrical initial distribution of the lost injected particles on the vertical phase space given on Fig. 23 implies the mentioned vertical mismatch of the injected beam.

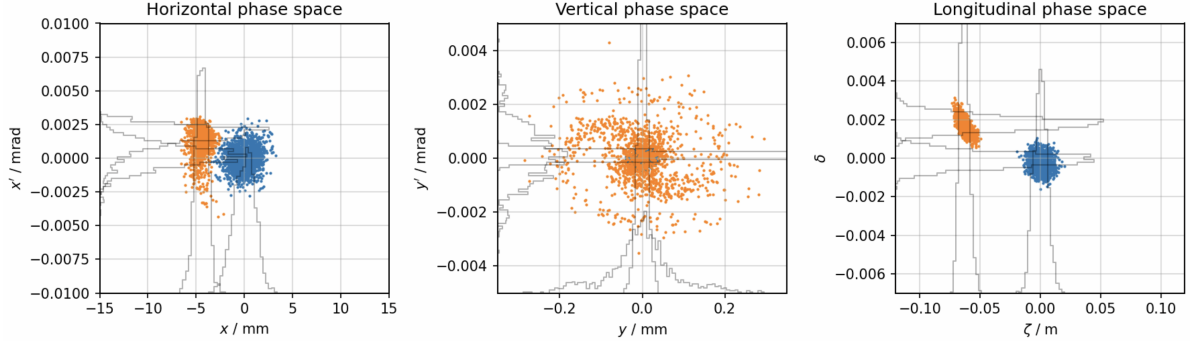


Figure 22: Observed filamentation in vertical phase space with $x = 1.9$ mm betatron offset and $\delta_{offset} = -0.5\%$ momentum offset. Injected particles are in orange color and circulating particles are in blue color.

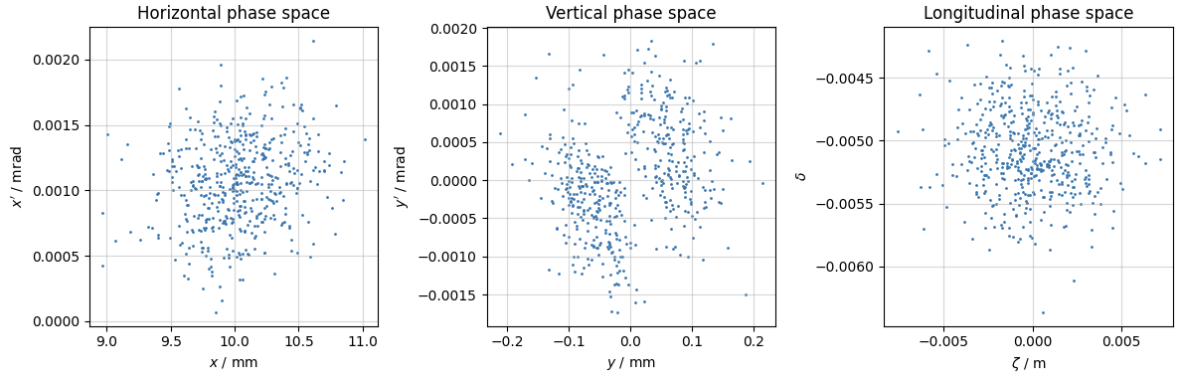


Figure 23: Initial position of lost injected particles.

In the rest of this study off-energy twiss parameters at the injection point was used for the injected beam. Using the off-energy twiss parameters, no filamentation was observed during tracking and the initial distribution of injected particles became symmetrical in the vertical phase space.

4.3 Parameter Scan for Betatron and Momentum Offset

To find the optimal betatron and momentum offset values, a parameter scan involving 14 jobs was performed on CERN's batch service. Each betatron offset and the corresponding momentum offset were chosen to ensure a 2.8 mm separation between the 5σ beam envelopes of the injected and circulating beams at the injection point. Beam parameters used in these jobs are presented on Tab. 3. Parameters used at each job and resultant injection efficiency are presented on Tab. 4.

Table 3: Beam parameters used for betatron and momentum offset optimization

	ϵ_x (nm)	ϵ_y (pm)	σ_z (mm)	σ_δ (10^{-4})
Circulating Beam	0.71	1.90	5.57	3.90
Injected Beam	0.122	2.00	2.43	3.90

Table 4: Parameter scan for 14 different betatron and momentum offset values. In total 1500 injected particles were tracked.

Job ID	Betatron Offset (mm)	Momentum Offset (%)	Lost Particle Number	Injection Efficiency (%)
0	-2.54	0.450	56	96.3
1	-2.12	0.475	45	97.0
2	-1.70	0.500	25	98.3
3	-1.28	0.525	17	98.9
4	-0.86	0.550	36	97.6
5	-0.45	0.575	73	95.1
6	-0.03	0.600	167	88.9
7	0.17	-0.600	55	96.3
8	0.53	-0.575	21	98.6
9	0.89	-0.550	8	99.5
10	1.26	-0.525	4	99.7
11	1.64	-0.500	16	98.9
12	2.03	-0.475	40	97.3
13	2.42	-0.450	85	94.3

4.4 Scan for Injected Beam Vertical Emittance

The injection repetition time affects the vertical emittance of the injected beam. Therefore, it is necessary to study injection efficiency across a range of possible values. To this end, a parameter scan for vertical emittance, consisting of 74 jobs, was performed on CERN's batch service. The injection efficiency was evaluated at vertical emittance values ranging from 2pm to 38pm for two injection schemes with different betatron and momentum offsets. The results are presented in Fig. 24. It was observed that the rate of decrease in injection efficiency with increasing vertical emittance depends significantly on the injection scheme. This observation can be explained by the asymmetry in the off-momentum dynamic aperture of the lattice with the injection optics, as shown in Fig. 11.

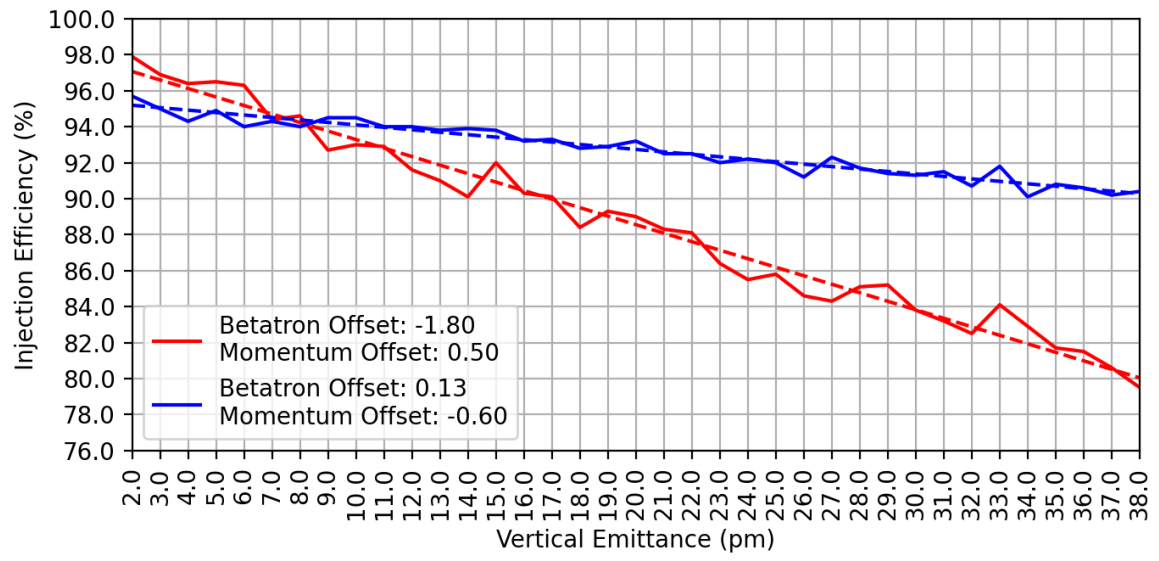


Figure 24: Injection efficiency vs vertical emittance of the injected beam with corresponding linear fits applied.

5 Conclusion

Several aspects of the FCC-ee top-up injection scheme in Z mode were investigated through particle tracking. The transverse and longitudinal damping times were analyzed for lattices with and without injection optics, revealing no significant impact of the injection optics on these damping times. Similarly, the transverse on-momentum dynamic aperture was examined, and once again, no substantial effect of the injection optics was detected. However, the previously designed injection optics were found to have a significantly high impact on the transverse off-momentum dynamic aperture of the collider lattice and nonlinear dispersion at the injection point. A new method was developed specifically to study this nonlinear dispersion.

Given the observed reduction in off-momentum aperture, the feasibility of a hybrid on-off axis injection scheme was explored. The study demonstrated the importance of using off-energy Twiss parameters for the injected beam, particularly in the vertical plane. A parameter scan was conducted to optimize the betatron and momentum offsets for the hybrid injection scheme, achieving a maximum injection efficiency of 99.7% with a 1.26 mm betatron offset and a -0.525% momentum offset. Finally, another parameter scan was performed to assess the impact of vertical emittance on injection efficiency. It was observed that the rate of decrease in injection efficiency with increasing vertical emittance is highly dependent on the chosen betatron and momentum offsets.

References

- [1] A. Abada et al. Fcc-ee: The lepton collider. *The European Physical Journal Special Topics*, 228(2):261–623, Jun 2019.
- [2] Paul Collier. Synchrotron phase space injection into LEP. *16th Biennial Particle Accelerator Conference and International Conference on High-Energy Accelerators, Dallas, TX, USA, 1 - 5 May 1995*, pp.551-553, 1996.
- [3] Paul Collier and G Roy. Injection and acceleration with physics optics in LEP. *5th European Particle Accelerator Conference*, 1996.
- [4] European Strategy Group. The European Strategy for Particle Physics Update 2013. La stratégie européenne pour la physique des particules Mise à jour 2013. 16th Session of European Strategy Council. Technical report, CERN, 2013.
- [5] European Strategy Group. 2020 Update of the European Strategy for Particle Physics (Brochure). Technical report, CERN, Geneva, 2020.
- [6] Giovanni Iadarola et al. Xsuite: An Integrated Beam Physics Simulation Framework. *JACoW*, HB2023:TUA2I1, 2024.
- [7] S Y Lee. *Accelerator Physics*. World Scientific, Singapore, 1999.
- [8] T. Mori et al. Design Study of Beam Injection for SuperKEKB Main Ring. In *Proc. IPAC'12*, pages 2035–2037. JACoW Publishing, Geneva, Switzerland, 2012.
- [9] S. Ogur, K. Oide, Y. Papaphilippou, D.N. Shatilov, and F. Zimmermann. Bunch Schedules for the FCC-ee Pre-injector. In *Proc. 9th International Particle Accelerator Conference (IPAC'18), Vancouver, BC, Canada, April 29-May 4, 2018*, number 9 in International Particle Accelerator Conference, pages 79–82, Geneva, Switzerland, June 2018. JACoW Publishing. <https://doi.org/10.18429/JACoW-IPAC2018-MOPMF001>.
- [10] Dr Katsunobu Oide. Ghc optics and collider parameters. FCC Week 2024, 2024.
- [11] Helmut Wiedemann. *Synchrotron Radiation*. Springer Berlin Heidelberg, Berlin, Heidelberg, 2003.
- [12] Sen Yue. Injection optics for 4ip lattice. 175th FCC-ee Optics Design Meeting & 46th FCCIS WP2.2 Meeting, 2024.